communications materials

Article

https://doi.org/10.1038/s43246-024-00569-2

Stabilization of P2 layered oxide electrodes in sodium-ion batteries through sodium evaporation

Check for updates

Maider Zarrabeitia [1,2,3], Iñigo Salazar [3,4], Begoña Acebedo [3,5] & Miguel Ángel Muñoz-Márquez [6,7]

Sodium-ion batteries are well positioned to become, in the near future, the energy storage system for stationary applications and light electromobility. However, two main drawbacks feed their underperformance, namely the irreversible sodium consumption during solid electrolyte interphase formation and the low sodiation degree of one of the most promising cathode materials: the P2-type layered oxides. Here, we show a scalable and low-cost sodiation process based on sodium thermal evaporation. This method tackles the poor sodiation degree of P2-type sodium layered oxides, thus overcoming the first irreversible capacity as demonstrated by manufacturing and testing all solid-state Na doped-$Na_{\sim 1}Mn_{0.8}Fe_{0.1}Ti_{0.1}O_2$ || PEO-based polymer electrolyte || Na full cells. The proposed sodium physical vapor deposition method opens the door for an easily scalable and low-cost strategy to incorporate any metal deficiency in the battery materials, further pushing the battery development.

Sodium-ion batteries (SIBs) are being considered as electrochemical energy storage devices for electric vehicles and large-scale stationary applications that could complement $LiFePO_4$ (LFP)-based lithium-ion batteries (LIBs) (https://www.catl.com/en/news/665.html). However, the energy density and long-term stability of SIBs must be improved for this technology to be more competitive in the market while becoming a solid alternative to other technologies that require critical raw materials. In this context, the electrochemically active materials are the bottleneck in terms of energy density for SIBs[1].

Among positive electroactive materials, the sodium layered oxides, with the general formula Na_xTMO_2 (TM = transition metal/s), are the best candidates in terms of high-energy density, scalability, and sustainability [2]. Sodium layered oxides can be classified considering the crystallographic site of sodium and the number of MO_2 layers in the unit cell. The most studied layered oxides are based on the O3-type and P2-type structures. The letter represents the sodium ions' crystallographic site (O = octahedral and P = trigonal prismatic), and it is followed by the number of MO_2 layers in the unit cell.

In general, the O3-type sodium layered oxides exhibit poor long-term stability due to the multiple phase transitions upon cycling. Meanwhile, the P2-type ones show superior rate capability and cycling stability, and appropriate specific capacity [3]. Besides, they can be easily synthesized and are considered environmentally friendly since abundant elements, such as manganese and iron, are their main constituents. However, their practical application is hindered due to the initial irreversible capacity, which is nested in the sodium deficiency of the material ($x \leq 0.67$ Na). This irreversibility, in combination with the most used anode, the sodium-free hard carbon, further amplifies the energy density problems of SIBs[4].

Hard carbon is a sodium-free negative electrode, and when combined with the sodium-deficient P2-type layered oxide, results in a full cell with significantly reduced first-cycle capacity and, in turn, specific energy density[5]. Therefore, using P2-type sodium layered oxide materials as cathode requires increasing the cathode mass to compensate for the first irreversible capacity of the sodium full cell. The excess cathode material, which remains inactive along further electrochemical cycles, significantly reduces the SIB energy density while increasing the cell cost (note that the cathode is around 1/3 of the total battery cost)[6].

One of the most accepted and used strategies to solve the sodium deficiency problem is chemical sodiation, which consists of the incorporation of a sodium-based sacrificial salt into the P2-based positive electrode[7]. At high voltage ($\geq$4.0 V vs. Na/Na^+), and mainly during the first cycles, the sacrificial salt is decomposed while releasing sodium ions and gas. The formers will incorporate into the cathode, partially solving the sodium deficiency problem, whilst the gas formation will increase the internal cell

[1]Helmholtz Institute Ulm (HIU), Helmholtzstrasse 11, 89081 Ulm, Germany. [2]Karlsruhe Institute of Technology (KIT), P.O. Box 3640, 76021 Karlsruhe, Germany. [3]Centre for Cooperative Research on Alternative Energies (CIC energiGUNE) Basque Research and Technology Alliance (BRTA) Alava Technology Park, Albert Einstein 48, 01510 Vitoria-Gasteiz, Spain. [4]Departamento de Física Aplicada II, Universidad del País Vasco UPV/EHU, 48940 Leioa, Spain. [5]Department of Organic and Inorganic Chemistry, Universidad del País Vasco (UPV/EHU), P.O. Box 664 Bilbao, 48080, Spain. [6]School of Science and Technology – Chemistry Division, University of Camerino, Via Madonna delle Carceri, 62032 Camerino, Italy. [7]National Reference Center for Electrochemical Energy Storage (GISEL) – INSTM, Via Giusti 9, 50121 Firenze, Italy. e-mail: miguel.munoz@unicam.it

Table 1 | Experimental parameters

Sample	I (A)	t (h)	Normalized Na deposition rate (nm h^{-1} ± 10%)
Na-doped NMFTO-01	9	19	184
Na-doped NMFTO-02	11	19	230
Na-doped NMFTO-03	12	19	410
Na-doped NMFTO-04	11	20	270

Current and evaporation time applied to the Na evaporation source to obtain four different Na-doped P2-NMFTO electrodes and Na evaporation rate normalized to the sample to source distance.

pressure, inducing electrode cracking, which is detrimental to long-term performance. Nevertheless, several sacrificial salts have been proposed recently, such as NaN_3[8,9], Na_3P[10], Na_2CO_3[11], $Na_2C_2O_4$[12], $Na_2C_4O_4$[13], and $Na_2C_3O_5$[5], as sodiation strategy to overcome the first irreversible capacity of P2-type sodium layered oxides.

The nitrogen- and phosphorous-based sacrificial salts, i.e., NaN_3 and Na_3P, overcome the first irreversible capacity. For example, adding 5% of NaN_3 to P2-$Na_{0.67}Mn_{0.5}Fe_{0.5}O_2$ reduces the irreversible capacity by 54%, thus enhancing the reversible capacity[8]. However, NaN_3 and Na_3P exhibit severe safety issues. NaN_3 is a toxic compound that is thermally unstable and can undergo explosive reaction with violent release of N_2 gas[9]. In addition, NaN_3 can also react with transition metals, leading to explosive sub-products. Meanwhile, Na_3P can release very dangerous sub-products such as phosphine[14].

Among all the sacrificial salts, the carbon-based Na_2CO_3, $Na_2C_4O_4$, and $Na_2C_3O_5$ have been demonstrated to reduce the irreversible capacity of P2-type layered oxides. However, this is accomplished by adding a high amount of sacrificial salt, which considerably reduces the amount of active material[5,13]. In addition, despite their easy manipulation and safety, the gas formation cannot be avoided upon reaction, and all reported sacrificial salts release O_2 and/or CO_2 gas during their decomposition, which results in crack formation on the electrode. At the same time, the gas reacts with the hard carbon negative electrode, triggering the electrolyte decomposition and decreasing the battery cycle life.

Finally, Oh et al. have reported on the thermal decomposition of $NaBH_4$ to pre-sodiate the hard carbon anodes and reduce the initial irreversible capacity[15]. However, the use of this method in positive electrodes is not clear enough.

Despite the extended use of sacrificial salts, this chemical method is only one possible approach for sodiation. Indeed, the physical vapor deposition (PVD) techniques could provide the required additional sodium to sodium-deficient electroactive materials for SIBs by means of an easily scalable and safe method. However, to the best of our knowledge, a physical vapor deposition route has never been carried out before. Na evaporation protocol, as reported here, is a fully safe method since no gas is released, and the sealed Na source can be manipulated in air prior to installation in the evaporation stage. In addition, a highly controlled and homogeneous Na layer can be deposed over the electroactive material. Besides, the proposed Na evaporation method is an easily scalable and highly efficient strategy that can be integrated into current battery production lines. Indeed, several PVD methods are currently used at the industrial level for metal deposition[16], such as thermal evaporation[17], direct current (DC) magnetron sputtering[18], high-power impulse magnetron sputtering (HiPIMS)[19], e-beam evaporation[20], and pulsed laser deposition (PLD)[21]. In roll-to-roll setup, metallization methods based on thermal evaporation can reach processing speeds higher than 10 m s^{-1} [22], well above current electrode processing speeds. In terms of coating thickness, high-rate PVD methods can deposit up to 0.1 µm s^{-1} [16]. At the same time, the vacuum levels used for PVD methods are compatible with air-sensitive battery materials and can guarantee the adequate preservation of the electroactive material properties. The application of PVD methods in mass production processes is a reality with a low impact on the cost of the final product. Indeed, candy wrap, crisps bags, and many other metalized plastic films are produced by means of PVD technology with retail costs below 1000 € ton^{-1} of finished product.

In this case, the sodium-deficient P2-$Na_{0.67}Mn_{0.8}Fe_{0.1}Ti_{0.1}O_2$ (P2-NMFTO) layered oxide was selected to integrate its sodium deficiency by means of thermal evaporation at the electrode level; in other words, a material modification strategy focused on solving the severe initial Coulombic efficiency problems. This P2 layered oxide is an excellent positive electrode for SIBs since it is mainly composed of non-toxic and earth-abundant elements, mainly manganese doped with 10% iron and titanium[23]. The latter buffers the Mn^{3+} Jahn-Teller distortions, providing structural reversibility upon electrochemical cycling while enhancing the cycle life by up to 83%[24]. It will be shown that after sodium evaporation, the resulting Na-doped-$Na_{\sim 1}Mn_{0.8}Fe_{0.1}Ti_{0.1}O_2$ (Na-doped NMFTO) delivers a specific capacity comparable to the one of P2-NMFTO, with improved (initial) Coulombic efficiencies and superior long-term stability in liquid- and solid-state-based electrolytes.

Results and discussion

Sodium deposition rate of the sodium evaporation process

The Na evaporation process on P2-NMFTO electrodes has been performed under vacuum by using commercially available Na sources. Considering that the Na source behaves as an ohmic resistor (see Supplementary Table 1 and Supplementary Fig. 1), the thickness of the sodium layer depends on the applied current, source-to-sample distance, and evaporation time. Therefore, the thickness of the deposited sodium layer can be determined by controlling the mentioned parameters. Table 1 summarizes the evaporation conditions, namely applied current (I) and the evaporation time (t), used during the preparation of the electrodes studied in this work. In the right column of Table 1, it is included the normalized sodium deposition rate as determined on commercial Si single-crystal substrates grown by the Czochralski method (Cz-Si), which are used as a reference. The normalized Na deposition rate is determined by taking into consideration source-to-sample distance that determines the area where the sodium atoms will be distributed, the thickness of the deposited sodium layer, and the time. This normalization does not depend on the sodium flux. In addition, please note that the sodium evaporation process has been performed under the same conditions and at the same time as for the P2-electrodes, taking into account the source-to-sample distance.

The normalized sodium deposition rate is the highest at the highest current density of 12 A and the lowest at the lowest current density of 9 A, in agreement with the ohmic behavior of the thermal evaporator. Therefore, obtaining large difference in thickness can be achieved by tunning the source-to-sample distance from 35 to 230 mm, which are the values used in this work. The normalized sodium deposition rate estimated for the two samples grown at 11 A is slightly different, 230 nm h^{-1} vs. 270 nm h^{-1}, but still overlaps within the experimental error of 10%.

Figure 1 displays the cross-section views of the single crystals collected by scanning electron microscopy (SEM). The Cz-Si single-crystals under the same Na evaporation conditions of Na-doped NMFTO-01 (Fig. 1a) and Na-doped NMFTO-04 (Fig. 1d), show some micro-particles in the cross-section area, which corresponds to surface species and sodium drawn during the cutting process of the sample for the cross-sectional analysis. This does not interfere with the determination of the thickness of the deposited sodium layer, which has been determined from the average values at different points of the sodium layer. The thickness value is used for the estimation of the normalized sodium deposition rate. The deposited sodium layer is rather homogeneous in all the Cz-Si in terms of surface coverage; however, it is rough in terms of thickness,

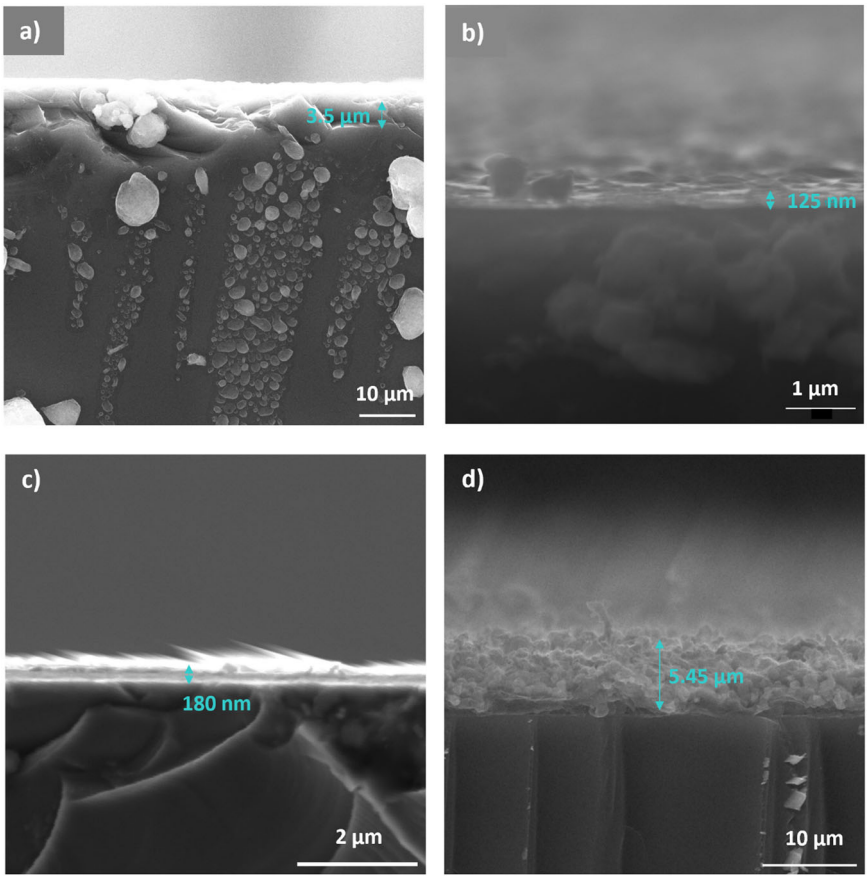

Fig. 1 | Sodium deposition rate. SEM cross-section images of the Cz-Si single-crystals under the same sodium evaporation conditions of **a** Na-doped NMFTO-01, **b** Na-doped NMFTO-02, **c** Na-doped NMFTO-03, and **d** Na-doped NMFTO-04 electrodes.

which will have some consequences when it comes to studying the Na-doped NMFTO electrodes, as it will be discussed later.

The samples grown with a low source-to-sample distance, namely Na-doped NMFTO-01 and Na-doped NMFTO-04, show a more dense sodium layer compared with the Na-doped NMFTO-02 and Na-doped NMFTO-03 electrodes that where produced using a larger source-to-sample distance. These results suggested that by increasing the sodium flux, as of Na-doped NMFTO-01 and Na-doped NMFTO-04, the sodium atoms can be better accommodated on the surface of the sample, forming a compact and homogeneous layer while lower sodium flux could result in slight nucleation, although the normalized Na deposition rate is higher. Electron dispersion spectroscopy (EDS) data of the samples indicate that the deposited overlayer is a mixture of carbon- and oxygen-containing Na-based compounds as well as Na metal, considering the C/O ratio (for element concentration, see Supplementary Fig. 2).

Surface morphology modification of the P2-electrodes after the sodium evaporation process

The effects of the sodium layer on the electrode surface morphology, have been studied on the Na-doped NMFTO-03 electrode by means of SEM (Fig. 2). The pristine surface of P2-NMFTO-03 (Fig. 2a) is smoother than the Na-coated one (Fig. 2b), suggesting the formation of a surface layer after evaporation, in agreement with the cross-section images of the Cz-Si samples shown in Fig. 1. At higher magnification, the Na-doped NMFTO-03 electrode (Fig. 2c, d) exhibits some particle clusters that might correspond to the formation of Na_2CO_3 and $NaCO_3R$ (R = alkyl chain), and Na metal particles, as later confirmed by X-ray photoelectron spectroscopy (XPS) and X-ray diffraction (XRD).

The cross-section analysis of the P2-NMFTO-03 electrode has also been performed (Supplementary Fig. 3) to eventually characterize the sodium layer. Unfortunately, the cross-section view does not allow us to determine the thickness of the sodium layer. Indeed, it is impossible to identify the presence of a sodium coating, probably due to the few nanometers thick formed overlayer and the evaporated sodium entering into the P2-NMFTO structure, as suggested by the structural change observed in XRD that will be discussed in the next section.

Surface and bulk chemistry modification after the sodium evaporation process

The surface of Na-doped NMFTO electrodes, as well as Cz-Si single-crystals, has been studied before and after the sodium evaporation process. The sodium concentration has been determined by means of XPS and EDS, and the surface chemical composition of the samples has been analyzed by means of XPS. This second step is crucial to verify the quality of the deposited sodium-based layer. After sodium evaporation on Cz-Si single-crystals, the XPS survey spectrum and EDS values clearly show that the sodium is deposited over the silicon substrate, in agreement with the cross-section images. Indeed, in the case of the XPS, the silicon peaks vanished, indicating full coverage of the substrate with a sodium layer at least 10-nm thick, while no bismuth signals were observed (see Supplementary Fig. 4), proving that only Na was evaporated. The minimum sodium layer thickness corresponds to the minimum coverage needed to prevent Si photoelectrons from escaping the substrate surface.

The same evaporation protocol used for the Cz-Si single-crystals has been used to prepare the Na-doped NMFTO electrodes. Figure 3 illustrates the XPS survey spectra of the Na-doped NMFTO electrodes before and after the sodium evaporation process as well as the calculated sodium atomic percentages in the inset. The atomic percentage variation of the other elements is summarized in Supplementary Fig. 5. In addition, the SEM and EDS values of the Cz-Si single-crystal prepared with the same protocol are illustrated.

The analysis of the Na 1s and Na KLL peaks in the XPS survey spectra collected from all Na-doped NMFTO electrodes clearly indicates that the sodium concentration increased in all cases after the sodium evaporation

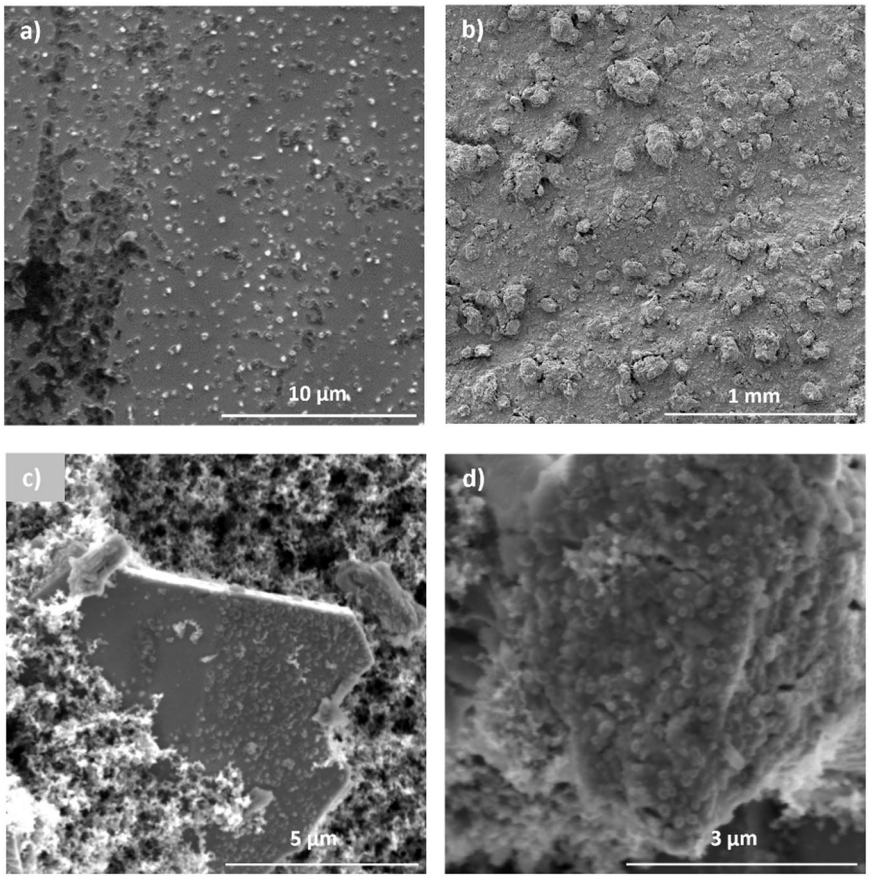

Fig. 2 | Surface morphology of P2-NMFTO and Na-doped NMFTO-03 electrodes. SEM images of **a** P2-NMFTO electrode at 10,000x magnification and Na-doped NMFTO-03 electrode at different magnifications **b** 100x, **c** 20,000x, and **d** 40,000x.

process, such 24.5, 11.4, 20.4, and 46.7 at% for Na-doped NMFTO-01, NMFTO-02, NMFTO-03, and NMFTO-04, respectively. In contrast, the F 1s and C 1s photoelectron peaks corresponding to electrode components, such as polyvinylidene fluoride (PVDF) binder and carbon Super C65 conductive additive, disappear after the sodium evaporation. In agreement with the EDS observations on the Cz-Si single-crystal reference samples, and again indicating a full coverage of the electrode surface with a homogeneous sodium layer at least 10-nm thick. It should be ruled out that the sodium concentration determined from EDS (24.1, 8.6, 17.5, and 39.9 at% for Na-doped NMFTO-01, NMFTO-02, NMFTO-03, and NMFTO-04, respectively) is slightly lower than those obtained from XPS due to the different sensitivity of the instrument. The XPS technique is highly surface-sensitive, while the EDS also proves the subsurface and near bulk region. Interestingly, the XPS and EDS results suggested that the sodium is mainly on the surface of the Na-doped NMFTO electrodes. However, it should not exclude the incorporation of sodium into the NMFTO structure, as confirmed below by XRD. Moreover, the sodium concentrations measured are in agreement with the sodium evaporation parameters used: the sodium coatings deployed at low source-to-sample distance, namely Na-doped NMFTO-01 and Na-doped NMFTO-04, increase their concentration when increasing the current. The same trend is observed for the coatings deployed at a high source-to-sample distance, i.e., Na-doped NMFTO-02 and Na-doped NMFTO-03. Once more, this indicates the importance of the source-to-sample distance parameter for the sodium evaporation process, resulting in more homogeneous and dense coatings when the Na flux is increased.

The increase in the atomic concentration of sodium in the electrode does not directly indicate that a pure sodium layer is formed. Indeed, the surface composition after sodium evaporation should be analyzed to understand the chemistry of the Na-doped NMFTO electrodes. The detailed analysis of the O 1s region XPS showed that besides Na metal, other compounds, such as carbonates, which are already observed in the pristine P2-NMFTO electrode (see "Before" spectra), were present on the sample surface (Fig. 4). Note that the Na KLL Auger peaks overlap with the C 1s signal since the Na-doped NMFTO electrodes show a high contribution of the former; the C 1s region was not used for characterization purposes.

Interestingly, the oxygen concentration increases after evaporation (Supplementary Fig. 5), as well as the sodium, while the carbon concentration decreases, indicating a modification of the surface chemistry after the process. The O 1s region has been thoroughly investigated to understand the chemical composition of the deposited surface layer. In all pristine P2-NMFTO electrodes, a small TM-oxide signal corresponding to the layered oxide (labeled as P2) is observed, along with more intense signals corresponding to Na_2CO_3 and $NaCO_3R$. This is consistent with the presence of a native passivation layer grown during the electrode preparation process that is rather thin and/or inhomogeneous and partially covers the pristine P2-$Na_{0.63}Mn_{0.8}Fe_{0.1}Ti_{0.1}O_2$ active material[25].

After sodium evaporation, the surface composition does not change for all the electrodes. However, the concentration of the species already observed in the pristine P2-NMFTO differs among Na-doped NMFTO electrodes Despite a significant increase of the sodium concentration, the presence of the P2 peak at ~530 eV and other high binding energy compounds after evaporation on the Na-doped NMFTO-02 and Na-doped NMFTO-03 samples would correspond to inhomogeneities on the thickness of the sodium layer. This is in agreement with the rather inhomogeneous sodium layer observed on the Cz-Si single-crystals coated under the same experimental conditions as the mentioned electrodes. Meanwhile, the P2 signal is not present on the samples coated with a higher flux of evaporated sodium atoms, namely Na-doped NMFTO-01 and Na-doped NMFTO-04, which indicates the formation of a homogeneous surface layer. These results suggest that increasing the sodium concentration is not the driving factor for obtaining a homogeneous coating.

Finally, it is observed that the outermost surface region of the Na-doped electrodes is mainly composed of Na_2CO_3 and, to a lower extent,

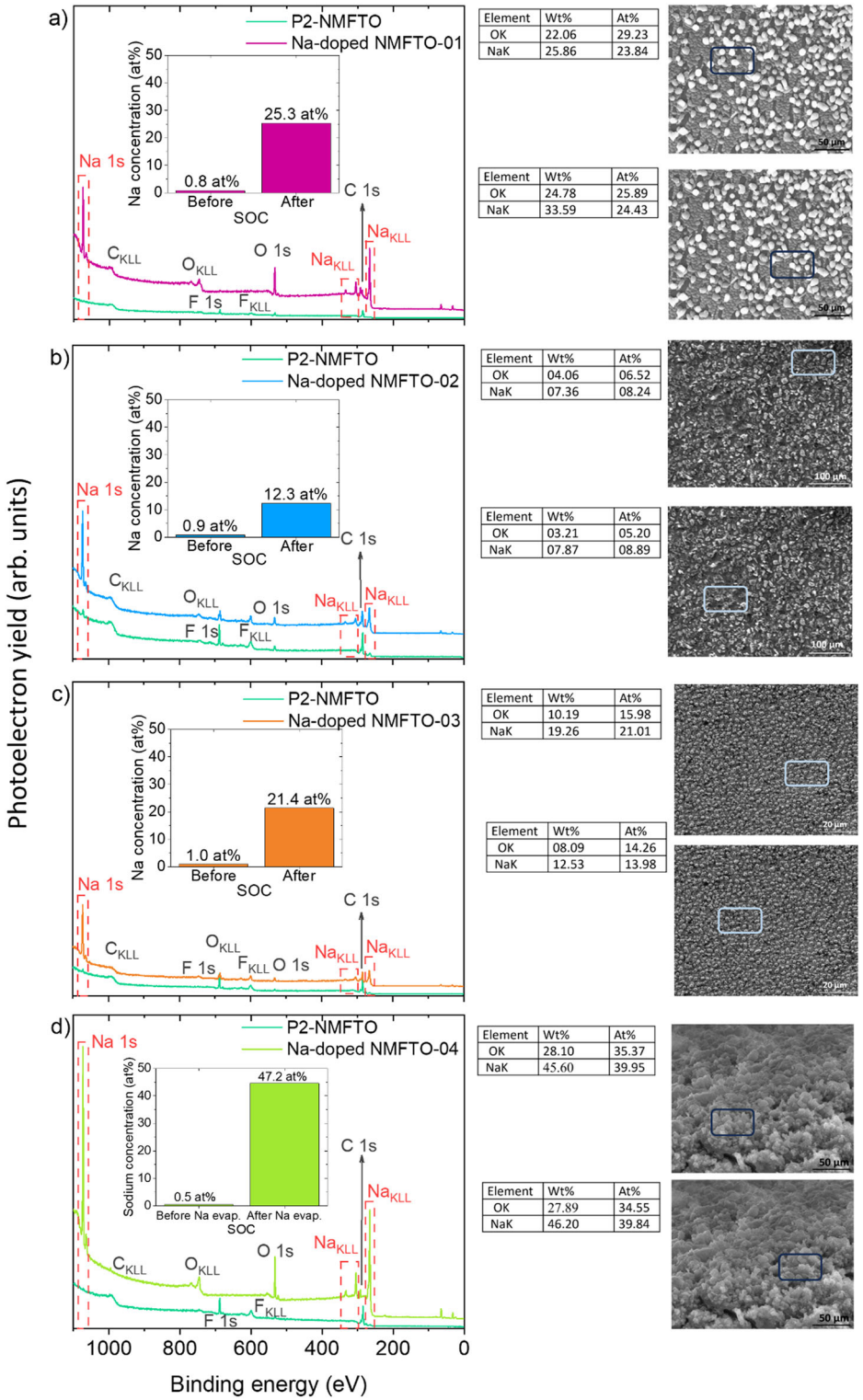

Fig. 3 | Surface and bulk chemistry of P2-NMFTO and Na-doped NMFTO electrodes. XPS survey spectra before and after sodium evaporation and surface SEM images and the corresponding EDS of **a** Na-doped NMFTO-01, **b** Na-doped NMFTO-02, **c** Na-doped-NMFTO-03, and **d** Na-doped NMFTO-04 electrodes. Inset, sodium atomic percentage was calculated for the corresponding electrode before and after the sodium evaporation process.

$NaCO_3R$. In contrast with the more evenly distributed composition of the pristine electrodes. The Na_2CO_3 concentration increase in the outermost surface region could be explained by the reaction of the evaporated Na metal with traces of H_2O and CO_2 present in the inert atmosphere that led to the formation of a carbonate-rich layer. Although the surface of the Na-doped P2-NMFTO electrodes contains a higher concentration of Na_2CO_3 due to the newly deposited sodium layer, similar reactivity as the pristine P2-NMFTO is expected. It should be noted that the chemistry of pristine and Na-doped NMFTO electrodes is similar as well as with the Na metal surface used as counter electrode[25]. Indeed, the outermost surface layer of the Na metal is mainly based on $NaCO_3R$, as confirmed by the C 1s, O 1s, Na 1s, and Na 2s photoelectron lines (Fig. 5).

In addition, the Na Auger parameter α(Na) further corroborates the presence of Na_2CO_3 in the outermost region of the Na metal. The α(Na) is a powerful approach to identifying the surface species due to its surface sensitivity because of the low kinetic energy and a short inelastic mean free path of the Na 1s photoelectrons[26]. The α(Na) can be defined as the energy gap between the binding energy of the Na 1s photoelectrons (1071.2 eV) and the kinetic energy of the Auger electrons (990.2 eV). The calculated α(Na) corresponds to Na_2CO_3 (2061.3 eV) and is in agreement with the

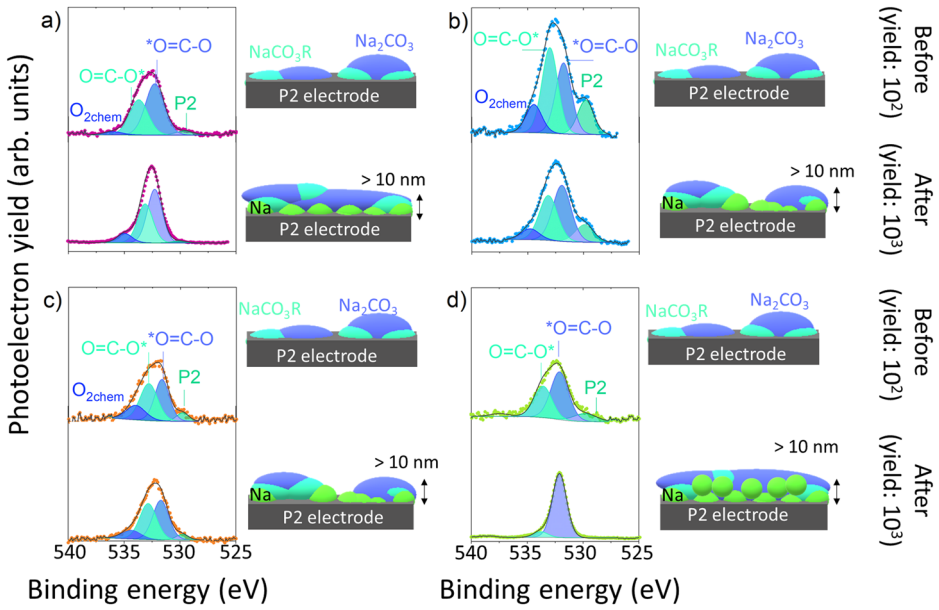

Fig. 4 | Surface chemistry of P2-NMFTO and Na-doped NMFTO electrodes. O 1s XPS region before and after sodium evaporation of **a** Na-doped NMFTO-01, **b** Na-doped NMFTO-02, **c** Na-doped-NMFTO-03, and **d** Na-doped NMFTO-04 electrodes along with the corresponding interfacial chemistry scheme.

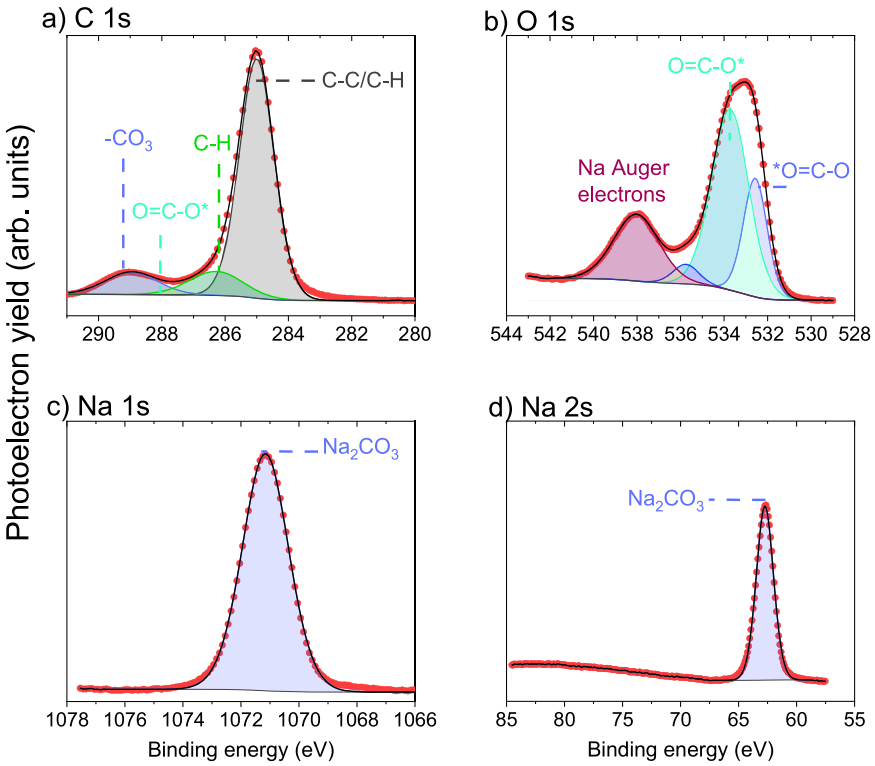

Fig. 5 | Surface chemistry of Na metal counter and reference electrode. a C 1s, **b** O 1s, **c** Na 1s, and **d** Na 2s XPS regions of the Na metal prepared inside the Ar glove box (O_2 <0.1 ppm, and H_2O <0.1 ppm).

EDS and XPS data[27]. Moreover, the lack of the Na metal plasmon on the Na 2s region indicates that the Na metal surface is homogeneously covered by sodium (alkyl) carbonates[28].

Nevertheless, this carbonate layer is found in the outermost surface region, as suggested by the XRD results and the sodium concentration values that point to the presence of metallic Na in the subsurface region. It is worth mentioning that the oxygen concentration increases by 10% after sodium evaporation, while the sodium concentration rises by more than 80%.

Structural modification after the sodium evaporation process

Considering that the source releases atomic sodium, an interaction of the highly reactive sodium atoms with the P2-layered oxide was expected. For this reason, an XRD study was carried out on the more interesting sample: Na-NMFTO-04, which is the one with the higher sodium concentration and homogeneous overlayer. The structural modifications of the sodium-evaporated P2-$Na_{0.67}Mn_{0.8}Fe_{0.1}Ti_{0.1}O_2$ electrode were investigated and compared with the pristine electrode (chemical composition determined by inductively coupled plasma spectroscopy, i.e., Na: 0.67, Mn: 0.75, Fe: 0.09, and Ti: 0.09). The purity of the pristine P2-NMFTO powder was previously confirmed by XRD Rietveld refinement, showing a hexagonal P2-type structure (space groups $P6_3/mmc$): for Rietveld refinement see Supplementary Fig. 6, the cell parameters and atomic positions are included in Supplementary Table 2. The XRD pattern of the pristine P2-NMFTO electrode displays the reflections of pure P2-type layered oxide (Fig. 6a).

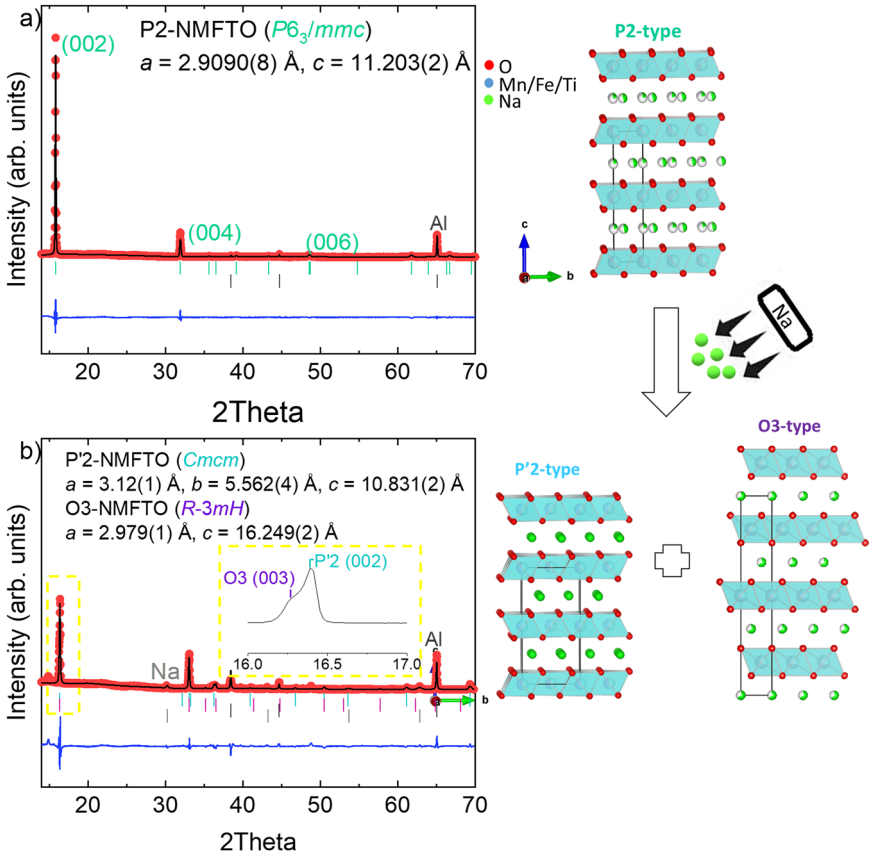

Fig. 6 | Structural characterization of materials. Le Bail refinement of XRD spectra from **a** pristine P2-NMFTO and **b** Na-doped NMFTO-04 electrodes. Experimental (red points), calculated (black line), difference curve (blue line), and Bragg positions (bars). Inset, a zoom of the main P'2 (cyan) and O3-type (purple) reflections. The corresponding crystallographic structure is displayed. Sodium (green), transition metals (blue), and oxygen (red) atoms.

Meanwhile, the Na-doped NMFTO-04 shows a clear modification of the structure (Fig. 6b): the reflections are consistent with the P'2- and O3-type layered oxides[29], indicating the formation of biphasic P'2/O3-type Na-doped NMFTO layered oxide. The formation of P'2- and O3-type phases indicates that the evaporated sodium not only covers the surface of the electrode but also incorporates into the structure. The formation of P'2-type is induced by the sodium ion occupying the trigonal prismatic site and distorting the MnO_6 octahedra caused by the formation of Jahn-Teller active Mn^{3+}. Meanwhile, the O3-type structure formation should be caused by a re-organization of the layer, which might be induced by a slight temperature increase and interaction with high-energy Na atoms during the sodium evaporation process under ultra-high vacuum conditions (10^{-8}–10^{-9} mbar). It should be noted that the pristine P2-type structure is unstable with a sodium content >0.7; a phase transformation is expected when incorporating evaporated sodium into the material's structure. Indeed, when trying to increase the sodium content above 0.7 by means of direct chemical synthesis, P'2-type Na_1TMO_2 layered oxides cannot be obtained[30]; instead, the reaction yields O3-type Na_1TMO_2 layered oxides.

The refinement of the XRD pattern can be used to roughly determine the fraction concentration of each phase. The estimation indicates that the P'2-type layered oxide is the main phase with around 33% while 14% corresponds to O3-type layered oxide. The remaining 30 and 23% fractions are Al from the current collector and Na metal, respectively.

Sodium liquid cells: electrochemical characterization of Na-doped NMFTO electrodes

The electrochemical performance of the Na-doped NMFTO electrodes in half cells has been tested using conventional liquid electrolyte, i.e., 1M $NaPF_6$ in ethylene carbonate:propylene carbonate (EC:PC) with 2wt% fluoroethylene carbonate (FEC), and compared with the pristine P2-NMFTO electrode (Fig. 7). The potential profiles of the first cycle prove the effectivity of the evaporated sodium layer as a sodium source for the cathode, resulting in enhanced first cycle reversible capacity. In other words, the pristine P2-NMFTO electrode suffers an irreversible capacity loss of 69 mAh g^{-1} during the first cycle (89 and 158 mAh g^{-1} charge and discharge capacity, respectively), while the Na-doped NMFTO electrodes show much lower irreversibility thanks to the sodiation strategy. The first cycle's reversibility is directly correlated with the sodium concentration deposited on the surface. The Na-doped NMFTO-03 and NMFTO-01 electrodes, which contain similar sodium content (around 25–20 at%), exhibit around 40 mAh g^{-1} irreversible capacity i.e., 98/147 mAh g^{-1} and 90/136 mAh g^{-1} of charge/discharge capacity, respectively. Meanwhile, the Na-doped NMFTO-02, with the lower sodium concentration, delivers an irreversible capacity of 45 mAh g^{-1}.

In addition, the potential profiles of Na-doped NMFTO electrodes are similar to the pristine P2-NMFTO, although the P2-phase shows a partial transformation to P′2- and O3-type structures. This has already been observed for other P2- and O3-type sodium layered oxides with the same composition[31,32]. It should be noted that, in this case, the phase transition of the P′2-type layered oxide is avoided within the selected voltage window. The similarity in the potential profile is also confirmed by the dQ/dV plots of the 1st, 25th, 50th, and 100th cycles, where no differences are observed (Supplementary Fig. 7), indicating similar electrochemical processes despite the higher initial reversible capacity due to the incorporation of the sodium by the evaporation method.

As XPS results indicate, the formed surface layer is also composed of Na_2CO_3, which could be responsible for the higher reversibility rather than the deposited sodium surface layer. Therefore, Na_2CO_3 was added as sacrificial salt to the P2-NMFTO electrode and tested in the same operating voltage range as the Na-doped NMFTO electrodes. The potential profile shows (Supplementary Fig. 8) a similar irreversible capacity to the pristine P2-NMFTO electrode. The Na_2CO_3 decomposition reaction is not observed in the applied operating voltage range. Note that when Na_2CO_3 behaves as sacrificial salt, an extra plateau at high voltage should be observed because Na and CO_2 gas are released[11].

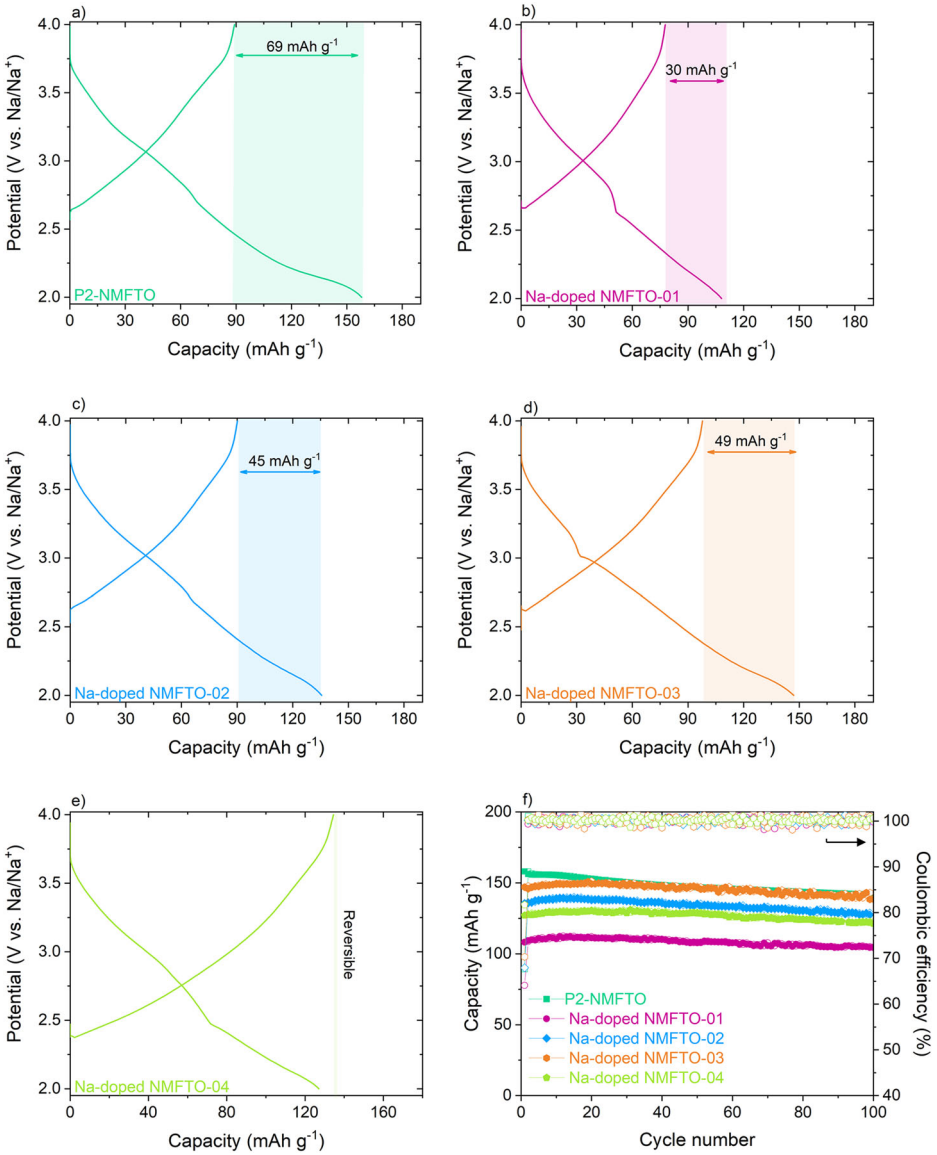

Fig. 7 | Electrochemical performance of P2-NMFTO and Na-doped NMFTO electrodes in liquid cells. Potential profile of the first cycle and the corresponding irreversible capacity of **a** P2-NMFTO, **b** Na-doped NMFTO-01, **c** Na-doped NMFTO-02, **d** Na-doped NMFTO-03, and **e** Na-doped NMFTO-04 electrodes. **f** Cycling performance of studied electrodes at 0.1C in the 2.0–4.0 V vs. Na/Na^+ operating voltage at 20 °C.

Surprisingly, the Na-doped NMFTO-04 electrode, where the highest sodium concentration is obtained with a very homogeneous surface layer in terms of composition and morphology, shows a complete reversible capacity in the first cycle (Fig. 7e). Even the first charge capacity slightly overcomes the first discharge (134 vs. 127 mAh g^{-1}, respectively). Other sodiation methods have never achieved this improvement[5,8–13], thus indicating that the sodium evaporation method is the best to overcome one of the main challenges of the sodium-based P2-layered oxides.

Regarding the specific capacities, the Na-doped NMFTO electrodes deliver lower capacity than the pristine P2-NMTFO, probably due to the increase of the interfacial resistance triggered by the carbonate-rich surface layer that ultimately hampers the sodium diffusion across the interphase. However, the carbonate-rich surface layer does not influence the long-term stability. Indeed, the capacity retention is improved for the Na-doped NMFTO electrodes. Even more, the samples with more homogeneous coatings, namely Na-doped NMFTO-01 and NMFTO-04, deliver the highest capacity retention over 100 cycles, 96.3% and 95.5%, respectively, followed by the less homogeneous coatings of Na-doped NMFTO-03 and Na-doped NMFTO-02 with 95.1 and 94.6%, respectively, while the P2-NMFTO exhibits only 89.8% capacity retention after 100 cycles. The better life cycle of the Na-doped NMFTO electrodes might be due to the formation of a biphasic structure (P'2/O3), which can stabilize the structure upon cycling, as was observed for other P2/O3 layered oxides[29,33]. However, it cannot be excluded the possible influence of the formed sodium layer, which could source more sodium during the interface formation while preventing the sodium consumption for the electrolyte and forming a good cathode electrolyte interphase (CEI). Therefore, further investigation should be carried out after cycling to understand the differences between the pristine P2-NMFTO and Na-doped NMFTO.

In addition, the Coulombic efficiency is also affected. As mentioned above, the main difference can be observed in the first cycle, showing higher first Coulombic efficiency for the Na-doped electrodes than the pristine P2-NMFTO, i.e., 100% of the Na-doped NMFTO-04, followed by NMFTO-01 (71.9%), NMFTO-03 (66.6%), NMFTO-02 (66.5%), and P2-NMFTO (56.4%). In the second cycle, the Coulombic efficiency increases up to 99.9% in the pristine P2-NMFTO, as well as on the Na-doped NMFTO electrodes with homogeneous and high sodium content layers, such as Na-doped-NMFTO-01 and NMFTO-04. Meanwhile, the Na-doped NMFTO-02 and NMFTO-03 deliver unstable Coulombic efficiency upon cycling (see Fig. 7f). These values suggested that the sodium-rich layer might prevent the electrolyte decomposition, also behaving as artificial CEI and/or providing sodium to the system upon electrochemical cycling (not only in the first cycles).

The electrochemical performances of the studied Na-doped NMFTO electrodes clearly show that the PVD of sodium enhanced the

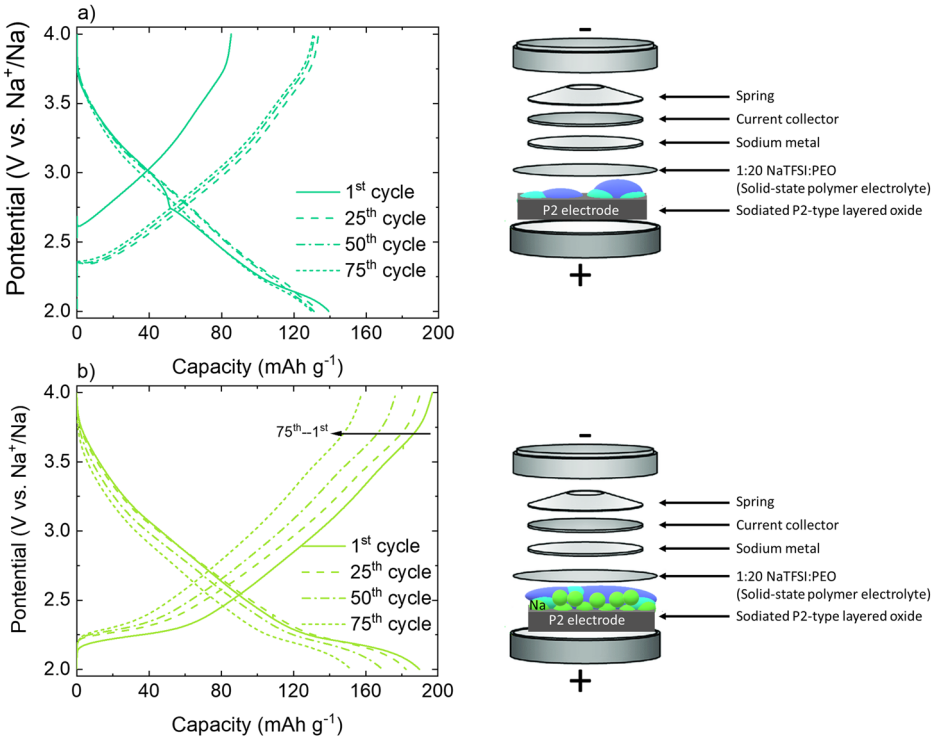

Fig. 8 | Solid-state sodium-metal cells. Potential profile of the 1st, 25th, 50th, and 75th cycles using as electrolyte PEO:NaTFSI solid-state polymer and as working electrode **a** P2-NMFTO or **b** Na-doped NMFTO-04. The all-solid-state sodium-metal cells were run at 0.1C in the 2.0–4.0 V vs. Na/Na^+ operating voltage at 70 °C.

electrochemical properties in terms of first irreversible capacity, (initial) Coulombic efficiency, and lifetime on the promising P2-based cathode material via the safe, low-cost, and scalable method, not introducing inert material to the electrode composition and in turn not increasing the cost of the SIBs.

Solid-state sodium-metal cells: electrochemical characterization of Na-doped NMFTO electrodes

The presodiation strategy of P2-layered oxides by thermal evaporation of sodium has also been demonstrated in all-solid-state sodium metal cells as proof of concept, using poly(ethylene oxide) (PEO):sodium trifluoromethanesulfonate (NaTFSI) ($EO/Na^+ = 20$ weigh ratio) polymer electrolyte operating at 70 °C. In this case, the electrochemical tests have been performed with the best Na-doped electrode, namely Na-doped NMFTO-04. The 1st, 25th, 50th, and 75th potential profiles of both pristine and Na-doped-NMFTO-041 electrodes in all-solid-state cells are illustrated in Fig. 8.

The first cycle potential profile of both electrodes is in agreement with those observed in liquid electrolyte sodium-metal cells. The pristine P2-NMFTO electrode exhibits 54 mAh g^{-1} of irreversible capacity in the first cycle. Interestingly, the first irreversible capacity of pristine P2-NMFTO in solid-state sodium-metal cells is slightly lower (15 mAh g^{-1}) than in liquid cells. This might indicate that the decomposition of liquid electrolytes also contributes to the irreversible capacity due to the formation of the CEI[25].

Meanwhile, as in liquid cells, the Na-doped NMFTO-04 shows a fully reversible capacity due to the sodium-rich layer formed by the sodium evaporation approach behaving as a sodium reserve. Furthermore, the all-solid-state sodium-metal cell delivers higher specific capacity than the cells with pristine NMFTO, i.e., 168 vs. 131 mAh g^{-1}. The higher delivered specific capacity might be due to the sodium reserves formed in the surface layer boosting the electrochemical performance. Nevertheless, further optimization should be carried out to enhance the capacity retention of Na-doped NMFTO-04 in all-solid-state sodium-metal cells.

The electrochemical performance enhancement of Na-doped NMFTO-04 ‖ PEO:NaTFSI ‖ Na has been compared with other reported works[34,35], where sodium layered oxides are used as cathode and PEO:Na-salt as polymer electrolytes. The Na-doped NMFTO-04 ‖ PEO:NaTFSI ‖ Na delivers an initial discharge capacity of 182 mAh g^{-1}, with a capacity retention of 94% (after 50 cycles) at 0.1C and 70 °C, while the P2-$Na_{0.67}Ni_{0.33}Mn_{0.67}O_2$ ‖ PEO:NaFSI (sodium bis(fluorosulfonyl)imid), $EO/Na^+ = 20$) ‖ Na delivers around 70 mAh g^{-1} with a capacity retention of 85% (after 50 cycles) at 0.2C and 80 °C[34]. In addition, the fully sodiated $NaCu_{0.11}Ni_{0.22}Fe_{0.33}Mn_{0.33}O_2$ layered oxide is also tested in all-solid-state sodium-metal cells ($NaCu_{0.11}Ni_{0.22}Fe_{0.33}Mn_{0.33}O_2$ ‖ PEO:NaFNFSI (sodium (fluorosulfonyl) (*n*-nonafluorobutanesulfonyl), $EO/Na^+ = 15$) ‖ Na, delivering an initial discharge capacity of 122 mAh g^{-1} at 0.1C and 80 °C[35]. These results suggest that the developed sodiation strategy, i.e., sodium evaporation at the electrode level, is an excellent approach for liquid and all-solid-state sodium-metal cells, overcoming previous results while providing a successful and suitable method to solve one of the main drawbacks of the P2-type sodium layered oxide electrodes in turn, enhancing the performances of sodium-based batteries.

Conclusions

Here is reported a scalable and low-cost presodiation methodology that solves the low sodiation degree of P2-type sodium layered oxides while eliminating the first irreversible capacity problems and increasing the capacity retention after long cycling. The sodium-deficient P2-type electrodes have been sodiated by means of thermal evaporation of sodium, resulting always in electrodes with higher reversible capacity than the pristine P2-NMFTO. The coating of a homogeneous sodium layer leads to Na-doped NMFTO electrodes that display full first-cycle reversible capacity, good specific capacity of 127 mAh g^{-1}, excellent Coulombic efficiency of 99.9%, and a capacity retention of 96.3% after 100 cycles when assembled in liquid electrolyte-based sodium-metal cells. Furthermore, the flexibility of the sodium evaporation approach is demonstrated by manufacturing all-solid-state Na-doped-$Na_{\sim 1}Mn_{0.8}Fe_{0.1}Ti_{0.1}O_2$ ‖ PEO:NaTFSI-based polymer electrolyte ‖ Na cells, which exhibit 100% of initial reversible capacity and a specific capacity of 168 mAh g^{-1} at 50th cycle, which corresponds to an average voltage of 2.6 V vs. Na metal and an estimated energy density of 440 Wh kg^{-1} (considering the cathode weight) at coin cell level. The proposed new -to the best of our knowledge-, scalable, safe, and low-cost sodiation strategy is an excellent method to overcome one of the main issues of P2-type sodium cathode materials. Further investigations should be carried out to optimize the proposed methodology, as well as fully

understand the mechanism behind it. Nevertheless, the excellent results obtained by this methodology can be applied to other materials that could significantly enhance the electrochemical performance of sodium-based batteries, thus accelerating the development of next-generation SIBs.

Methods

Synthesis of P2-$Na_{0.67}Mn_{0.8}Fe_{0.1}Ti_{0.1}O_2$

P2-$Na_{0.67}Mn_{0.8}Fe_{0.1}Ti_{0.1}O_2$ was synthesized by solid-state method, mixing in stoichiometric amounts anhydrous Na_2CO_3 (≥99.5%, Scharlab), Mn_2O_3 (98%, Alfa Aesar), Fe_2O_3 (97%, Alfa Aesar), and TiO_2 (99.5%, Sigma Aldrich), and annealed at 1000 °C for 6 h under ambient air. The obtained black powder was transferred to a glove box during cooling to avoid surface contamination.

Degassing and sodium evaporation

The sodium source $BiNa_3$ (AlfaVakuo e.U.) is sealed with indium so it can be safely handled and mounted in ambient air conditions (https://alfavakuo.eu/products/mvs/#Alloy). The sodium source is connected to two conductor bars (Supplementary Fig. 9a). Besides, these two bars are also connected to an external current supply machine. The sodium source was inserted in an ultra-high vacuum (10^{-8} mbar) chamber (Supplementary Fig. 9b) for evaporation. The indium seal was melted, driving through a current of 4–5 A for 1 h, following the procedure recommended by the supplier (https://alfavakuo.eu/products/mvs/#Alloy) to ensure that the seal was completely melted and any eventual surface impurities were decomposed. The sodium evaporation was carried out at the electrode level on P2-$Na_{0.67}Mn_{0.8}Fe_{0.1}Ti_{0.1}O_2$ electrodes (12-mm diameter disks) that were transferred to the ultra-high vacuum chamber. The sodium evaporation occurs at 900 °C under 10^{-6} Pa. Three different currents were applied to the sodium source: 9, 11, and 12 A during 19 or 20 h. The source was placed at two different distances from the sample to obtain two different fluxes of Na. Two samples were prepared at 35 mm from the Na source, and two samples were prepared at 230 mm from the Na source. The Na-doped $Na_{\sim1}Mn_{0.8}Fe_{0.1}Ti_{0.1}O_2$ electrodes were transferred to the glove box with an Ar-tight transfer holder, avoiding atmospheric contamination.

Morphological characterization

SEM images and EDS of the samples, i.e., P2-NMFTO, Na-doped NMFTO, and Cz-Si single-crystals before and after sodium evaporation, were collected using a Quanta 200 FEG-FEI model. Micrographs were acquired from the top and cross-section view.

Surface chemistry characterization

XPS technique was performed to analyze the surface chemistry of the samples. The pristine P2-NMFTO electrodes and the Cz-Si single crystals before and after the sodium evaporation process were measured. The Cz-Si single crystals were used as a reference. The electrodes were transferred from the glove box or sodium evaporation chamber to the XPS system via an Ar-filled transfer holder (the samples were never exposed to air). A non-monochromatic Mg Kα (hν = 1253.6 eV) X-ray source and Phoibos 150 XPS spectrometer equipped with a micro-channel plate and Delay Line Detector was used. The scans were acquired with an X-ray source power of 200 W, 20 eV pass energy (fixed analyzer transmission mode), and 0.1 eV energy step. The photoelectron binding energy was calibrated using the graphitic peak (-C-C- sp^2) at 284.4 eV as a reference[36]. The deconvolutions of the spectra were carried out with CasaXPS software, using a nonlinear Shirley-type background and 70% Gaussian and 30% Lorentzian profile function[37].

Structural characterization

The structural properties of P2-$Na_{0.67}Mn_{0.8}Fe_{0.1}Ti_{0.1}O_2$ powder and electrode, as well as Na-doped NMFTO electrodes, were investigated by XRD. Diffractograms were recorded on a Bruker Discover D8 instrument equipped with monochromatic Cu radiation ($K_{\alpha1}$ = 1.5406 Å) and a LYNXEYE-XE detector with a step size of 0.02°. The X-ray diffractograms were refined with the FullProf software, and the structures were drawn by VESTA[38,39].

Electrochemical characterization

80% P2-$Na_{0.67}Mn_{0.8}Fe_{0.1}Ti_{0.1}O_2$, 10% carbon Super C65 (Timcal), and 10% PVDF (6020 Solef®, Arkema Group) in *N*-methyl-2-pyrrolidone (NMP, Sigma Aldrich) were mixed. The slurry was cast on battery-grade Al foil and pre-dried under a dynamic vacuum at 120 °C overnight. 12-mm disk electrodes were punched and pressed at 4 tons for 30 s. The pristine P2-$Na_{0.67}Mn_{0.8}Fe_{0.1}Ti_{0.1}O_2$ (6.5 mg cm^{-2}) or Na-doped $Na_{\sim1}Mn_{0.8}Fe_{0.1}Ti_{0.1}O_2$ (7.0–11.0 mg cm^{-2}) electrodes were used as working electrode, and Na metal (Acros Organics, 99.8%) as counter and reference electrode in coin-type cells. Glass fiber (Whattman GF/D) was used as separator. The cells were assembled in an Ar-filled glove box (MBraun, H_2O, and O_2 <0.1 ppm). Two types of electrolytes were used: liquid and polymer electrolytes. The liquid electrolyte was 1M $NaPF_6$ in EC:PC (UBE) with 2wt.% FEC (UBE) and the polymer electrolyte was PEO (EO = 5,000,000): NaTFSI (Sigma Aldrich) in a weight ratio of 1:20 (EO:Na^+). The polymer electrolyte was deposited onto NMFTO electrodes (P2-NMFTO and Na-doped NFMTO-04) by spin-coating method (Ossila). The NaTFSI in PEO solution (0.8 mL) was dropped onto 12 mm NMFTO electrodes and rotated in three steps, i.e., first 30 s at 500 rpm, second 120 s at 1500 rpm, and third 120 s at 2500 rpm. Finally, the NMFTO electrodes coated with NaTFSI in PEO polymer electrolyte were dried under vacuum at 50 °C for 12 h. The galvanostatic measurements were carried out in a Maccor Series 4000 battery tester (USA) in the 2.0–4.0 V vs. Na/Na^+ voltage window at 0.1 °C at room temperature (20 °C) for liquid electrolyte-based cells and at 70 °C for all-solid-state sodium metal cells.

Data availability

Data is available from the corresponding author upon reasonable request.

Received: 24 October 2023; Accepted: 10 July 2024;
Published online: 23 July 2024

References

1. Abraham, K. M. How comparable are sodium-ion batteries to lithium-ion counterparts? *ACS Energy Lett*. **5**, 3544–3547 (2020).
2. Lui, Q. et al. Sodium transition metal oxides: the preferred cathode choice for future sodium-ion batteries? *Energy Environ. Sci.* **14**, 158–179 (2021).
3. Gonzalo, E., Zarrabeitia, M., Dreweet, N. E., López del Amo, J. M. & Rojo, T. Sodium manganese-rich layered oxides: potential candidates as positives electrode for sodium-ion batteries. *Energy Storage Mater*. 34, 682–707 (2021).
4. Meysami. S. An overview of hard carbon as anode materials for sodium-ion batteries. BatteyBitsEditors. https://medium.com/batterybits/an-overview-of-hard-carbon-as-anode-materials-for-sodium-ion-batteries-8db98fd60965 (2022).
5. Fernández-Ropero, A. J. et al. Improved sodiation additive and its nuances in the performance enhancement of sodium-ion batteries. *ACS Appl. Mater. Interfaces* **13**, 11814–11821 (2021).
6. Ortiz-Vitoriano, N., Drewett, N. E., Gonzalo, E. & Rojo, T. High performance manganese-based layered oxide cathodes: overcoming the challenges of sodium ion batteries. *Energy Environ. Sci.* **10**, 1051–1074 (2017).
7. Mariyappan, S., Wang, Q. & Tarascon, J. M. Will sodium layered oxides ever be competitive for sodium ion battery applications? *J. Electro Soc.* **165**, A3714–A3722 (2018).
8. Sing, G. et al. An approach to overcome first cycle irreversible capacity. *Electrochem. Commun.* **37**, 61–63 (2017).
9. Martinez De Ilarduya, J., Otaegui, L., López del Amo, J. M., Armand, M. & Singh, G. NaN_3 addition, a strategy to overcome the problem of sodium deficiency in P2-$Na_{0.67}[Fe_{0.5}Mn_{0.5}]O_2$ cathode for sodium-ion battery. *J. Power Sources* **337**, 197–203 (2017).
10. Zhang, B. et al. Insertion compounds and composite made by ball milling for advanced sodium-ion batteries. *Nat. Commun.* **7**, 10308 (2016).
11. Sathiya, M. et al. Dual stabilization and sacrificial effect of Na_2CO_3 for increasing capacities of Na-ion cells based on P2-Na_xMO_2 electrodes. *Chem. Mater.* **29**, 5948–5956 (2017).

12. Niu, Y.-B. et al. High-efficiency cathode sodium compensation for sodium-ion batteries. *Adv. Mater.* **32**, 2001419 (2020).
13. Shanmukaraj, D. et al. Highly efficient, cost effective, and safe sodiation agent for high-performance sodium-ion batteries. *ChemSusChem* **11**, 3286–3291 (2018).
14. Nie, J., Li, L. & Lu, J. Phosphorous: an anode of choice for sodium-ion batteries. *ACS Energy Lett.* **3**, 1137–1144 (2018).
15. Sam Oh, J. A. et al. High-performing all-solid-state sodium-ion batteries enabled by the presodiation of hard carbon. *Adv. Energy Mater.* **13**, 2300776 (2023).
16. Melentiev, R., Yudhanto, A., Tao, R., Vuchkov, T. & Lubineua, G. Metallization of polymers and composites: state-of-the-art approached. *Mater. Des.* **221**, 110958 (2022).
17. Arias, N. & Jaramillo, F. Highly reflective aluminum films on polycarbonate substrates by physical vapor deposition. *Appl. Surf. Sci.* **505**, 144596 (2020).
18. Baptista, A. et al. Wear characterization of chromium PVD coatings on polymeric substrate for automotive optical components. *Coatings* **11**, 555 (2021).
19. Zhang, D. et al. Comparative study on protective properties of CrN coatings on the ABS substrate by DMCS and HiPIMs techniques. *Surf. Coat. Tech.* **394**, 125890 (2020).
20. HeinB, J.-P. & Fietzke, F. High-rate deposition of thick aluminum coatings on plastic parts for electromagnetic shielding. *Surf. Coat. Tech.* **385**, 125134 (2020).
21. Liimatainen, J. et al. Ultra short pulsed laser deposition technology for industrial applications. *J. Mater. Sci. Eng. B* **5**, 196 (2015).
22. Stuart, B. W. et al. Linear electron beam assisted roll-to-roll in-vacuum flexographic patterning for flexible thermoelectric generators. *Coatings* **11**, 1470 (2021).
23. Han, M. H. et al. High-peformance P2-phase $Na_{2/3}Mn_{0.8}Fe_{0.1}Ti_{0.1}O_1$ cathode material for ambient-temperature sodium-ion batteries. *Chem. Mater.* **28**, 106–116 (2016).
24. Zarrabeitia, M. et al. Unraveling the role of Ti in the stability of positive layered oxide electrodes for rechargeable Na-ion batteries. *J. Mater. Chem. A* **7**, 14169–14179 (2019).
25. Zarrabeitia, M. et al. Towards stable electrode/electrolyte interface of P2-layered oxide for rechargeable Na-ion batteries. *ACS Appl. Mater. Interfaces* **11**, 28885–28893 (2019).
26. Muñoz-Márquez, M. A. et al. Composition and evaluation of the solid-electrolyte interphase in $Na_2Ti_3O_7$ electrodes for Na-ion batteries: XPS and Auger parameter analysis. *ACS Appl. Mater. Interfaces* **7**, 7801–7808 (2015).
27. Wagner, C. D., Riggs, W. M., Davis, L. E., Moulder, J. F. & Mullenberg, G. E. *Handbook of X-ray Photoelectron Spectroscopy* (Perkin-Elmer Corporation, 1979).
28. Kowalczyk, S. P., Ley, L., McFeely, F. R., Pollak, R. A. & Shirley, D. A. X-ray photoemission from sodium and lithium. *Phys. Rev. B* **8**, 3583–3585 (1973).
29. Maughan, P. A., Naden, A. B., Irvine, J. T. S. & Armstrong, A. R. Manipulating O3/P2 phase ratio in bi-phasic sodium layered oxides via ionic radius control. *Commun. Mater.* **4**, 6 (2023).
30. Yabuuchi, N. et al. P2-type $Na_x[Fe_{1/2}Mn_{1/2}]O_2$ made from earth-abundant elements for rechargeable Na batteries. *Nat. Mater.* **11**, 512–517 (2012).
31. Gonzalo, E. et al. Synthesis and characterization of pure P2- and O3-Na2/3Fe2/3Mn1/3O2 as cathode materials for Na ion batteries. *J. Mater. Chem. A* **2**, 18523–18530 (2014).
32. Han, M. H. et al. Synthesis and electrochemistry study of P2- and O3-phase $Na_{2/3}Fe_{1/2}Mn_{1/2}O_2$. *Electrochim. Acta* **182**, 1029–1036 (2015).
33. Zhou, D., Huang, W., Lv, X. & Zhao, F. A novel P2/O3 biphase $Na_{0.67}Fe_{0.425}Mn_{0.425}Mg_{0.15}O_2$ as cathode for high-performance sodium-ion batteries. *J. Power Sources* **421**, 147–155 (2016).
34. Qi, X. et al. Sodium bis(fluorosulfonyl)imide/poly(ethylene oxide) polymer electrolytes for sodium-ion batteries. *ChemElectroChem* **3**, 1741–1745 (2016).
35. Ma, Q. et al. A new Na[(FSO2)(n-C4F9SO2)N]-based polymer electrolyte for solid-state sodium batteries. *J. Mater. Chem. A* **5**, 7738–7743 (2017).
36. Biesinger, M. C. Accessing the robustness of adventitious carbon for charge referencing (correction) purposes in XPS analysis: insights from a multi-user facility data review. *Appl. Surf. Sci.* **597**, 153681 (2022).
37. Walton, J., Wincott, J., Fairley, P. & Carrick, N. A. *Peak Fitting with CasaXPS: A Casa Pocket Book* (Acolyte Science, 2010).
38. Rodríguez-Carvajal, J. Recent advances in magnetic structure determination by neutron powder diffraction. *Phys. B* **192**, 55–69 (1993).
39. Momma, K. & Izumi, F. VESTA: a three-dimensional visualization system for electronic and structural analysis. *J. Appl. Crystallogr.* **41**, 653–658 (2008).

Acknowledgements

M.Z. acknowledges the financial support from the BMBF Transition transfer project (FZK 03XP0533).

Author contributions

M.Z.: investigation, methodology, data analysis, visualization, and writing—original draft and editing. I.S.: investigation, data analysis, and review. B.A.: investigation, methodology, data analysis, visualization, and review. M.A.M.-M.: conceptualization, methodology, investigation, formal analysis, funding acquisition, project administration, supervision, and writing—review and editing.

Competing interests

The authors declare no competing interests.

Additional information

Supplementary information The online version contains supplementary material available at https://doi.org/10.1038/s43246-024-00569-2.

Correspondence and requests for materials should be addressed to Miguel Ángel Muñoz-Márquez.

Peer review information *Communications Materials* thanks Tianxi Liu and the other, anonymous, reviewer(s) for their contribution to the peer review of this work. Primary Handling Editors: Jet-Sing Lee.